

Phonon assisted light absorption and emission in cubic-Boron Nitride

Ashwin Pillai,¹ Elena Cannuccia,^{2,3} Aurelien Manchon,¹ Fulvio Paleari,⁴ and Claudio Attacalite¹

¹*Aix-Marseille Univ., CNRS, CINaM, Centre Interdisciplinaire de Nanoscience de Marseille, UMR 7325, Campus de Luminy, 13288 Marseille cedex 9, France*

²*Aix Marseille Univ, CNRS, PIIM, Physique des Interactions Ioniques et Moléculaires, UMR 7345, Marseille, France*

³*European Theoretical Spectroscopy Facility (ETSF)*

⁴*Centro S3, CNR-Istituto Nanoscienze, I-41125 Modena, Italy*

(*Electronic mail: ashwin.pillai@etu.univ-amu.fr)

(Dated: 23 February 2026)

Cubic boron nitride (cBN) is a wide-bandgap polymorph of boron nitride whose optical response remains only partially understood due to the coexistence of indirect electronic transitions and strong exciton-phonon coupling. Using first-principles many-body perturbation theory, we investigate the optical properties of cBN by combining GW quasiparticle corrections with Bethe-Salpeter equation calculations of excitonic effects. Phonon-assisted absorption and emission processes are explicitly included through the exciton-phonon coupling formalism. We find that phonon-mediated optical transitions provide a dominant contribution to both absorption and luminescence spectra, partially reconciling the discrepancy between the theoretical optical gap (≈ 11 eV) and experimental emission around 6–7 eV. Our results demonstrate the importance of including exciton-phonon interactions for the correct interpretation of experimental spectra, offering new insights into light emission in wide-bandgap materials.

I. INTRODUCTION

Boron nitride (BN) exhibits a rich polymorphism, encompassing phases ranging from the common hexagonal (hBN) and cubic (cBN) structures to more complex polytypes.¹ A significant challenge in the study of these materials is the frequent coexistence of different phases and the difficulty in obtaining perfectly pure samples. This complexity underscores the need for precise characterization techniques. While Raman spectroscopy is a widely used characterization tool in materials science, its utility for BN polymorphs is often limited due to the material's few active Raman modes and the deep UV band gap forcing nonresonant conditions. Consequently, luminescence spectroscopy emerges as a far more powerful and informative probe. The sensitivity of luminescence to electronic structure, defects, and stacking order makes it exceptionally well-suited for characterizing BN nanostructures, where it can reveal details that remain inaccessible to Raman scattering². For example, luminescence has proven to be a versatile tool, successfully distinguishing between different stacking sequences in the hexagonal phase³ and probing the effects of strain.^{4,5}

The past few years have witnessed intense experimental and theoretical interest in the luminescence properties of BN polymorphs.^{6–8} A unifying feature of most BN phases is their indirect band gap, meaning that luminescence typically arises from phonon-assisted transitions. Remarkably, despite this indirect nature, the luminescence efficiency in hBN has been shown to rival that of direct band gap materials.^{7,9} This high efficiency should be a consequence of the strong exciton-phonon coupling inherent to BN systems.^{10,11} Beyond hBN, luminescence has also been investigated in the wurtzite phase (wBN), though a direct comparison between experiment and theory remains challenging due to difficulties in synthesizing pure wBN.¹² Even in the direct band gap monolayer, luminescence studies are central in the debates over the origin of emission features, whether from direct or indirect transitions.^{13–17}

Within this family of polymorphs, cubic boron nitride (cBN) presents a particularly compelling and unresolved puzzle.^{18,19} As a thermodynamically stable phase at standard conditions, cBN has been synthesized primarily by chemical vapor deposition.^{18,19} Experimental optical measurements, including those under pressure,²⁰ consistently report an optical absorption onset around 6–7 eV.^{21–23} However, state-of-the-art theoretical calculations, which typically neglect the electron-phonon interaction, predict a much larger direct optical gap of approximately 11 eV.^{24–26} This significant discrepancy has been tentatively attributed to phonon-assisted indirect transitions, which could lower the observed absorption edge. Furthermore, the potential presence of hBN inclusions in experimental samples, which luminesce around 6 eV, may mask the intrinsic phonon-assisted emission signal from pure cBN.

From a theoretical point of view, exciton-phonon coupling has been mainly studied with different approaches: by finite difference methods^{4,12,27,28} and the direct calculation of microscopic exciton-phonon scattering amplitudes.^{3,15,16} In this work, we follow this second strategy to investigate the role of atomic vibrations in the optical response of cBN.

This work aims to address the long-standing discrepancy between theoretical predictions and experimental optical measurements in cubic boron nitride. While previous studies have investigated the optical properties of cBN either neglecting phonon effects²⁶ or treating phonon-assisted absorption without excitonic interactions²⁹, a unified first-principles description combining excitons and phonon scattering has so far been missing.

Here, we present a first-principles investigation of the optical absorption and luminescence of cBN that explicitly includes exciton-phonon coupling within a many-body perturbation theory framework. By combining GW quasiparticle corrections, Bethe-Salpeter equation calculations, and phonon-assisted optical processes, we assess the role of indirect excitonic transitions in shaping the optical spectra of cBN

and clarify their relevance for the interpretation of experimental observations.

This information is critical, given that cBN is a large-gap material where strongly bound excitons are expected and the coupling between excitons and phonons is known to be profound in other BN polymorphs.^{10,11} Furthermore, understanding exciton–phonon coupling in cBN has broader implications, particularly in light of recent studies on small polaron formation in doped cBN systems³⁰ and the reported observation of the electron–phonon Fano effect in cBN.³¹

The manuscript is organized as follows: in Sec. II we summarize all theoretical methods used in our calculations including the excitonic properties and the coupling with phonons; Sec. II C contains all computational parameters and code references used in this work; in Sec. III we present our results and compare them with the existing literature and experimental measurements; finally, in Sec. IV we draw conclusions and discuss future perspectives for this work.

II. THEORETICAL METHODS

The ground-state properties of cubic boron nitride are calculated within density functional theory (DFT), as implemented in the Quantum ESPRESSO package³². The experimental lattice parameter of 3.615 Å reported in Ref. 33 is used throughout. Vibrational properties and electron–phonon matrix elements are obtained using density functional perturbation theory (DFPT)³². All parameters that enter the calculation are reported in Sec. II C. Following our investigation of the ground-state properties, we shifted our focus to exploring the electronic structure and optical properties of cBN. To study the electronic bands of cBN, we diagonalized the Kohn-Sham (KS) Hamiltonian. However, as DFT is known to have limitations in accurately describing the electronic structure, including underestimating the electronic gap³⁴, we used Many-Body Perturbation Theory implemented in the Yambo code³⁵ to correct the KS eigenvalues. By doing so, we calculated the quasiparticle bandstructure as:

$$E_{n\mathbf{k}} = \varepsilon_{n\mathbf{k}}^{KS} + Z_{n\mathbf{k}} [Re\Sigma(\varepsilon_{n\mathbf{k}}^{KS}) - V_{n\mathbf{k}}^{xc}] \quad (1)$$

where $E_{n\mathbf{k}}$ are the corrected quasiparticle energies, $Z_{n\mathbf{k}}$ is the renormalization factor, $V_{n\mathbf{k}}^{xc}$ the exchange correlation KS potential and the self-energy Σ is calculated in the GW approximation $\Sigma = G_0W_0$ ³⁴, at frequency $\omega = \varepsilon_{n\mathbf{k}}^{KS}$. The screened interaction W_0 is calculated using the Godby-Needs plasmon-pole model.³⁶

Starting from the quasiparticle bandstructure we proceeded to calculate the optical response function, including the electron–hole interaction. To achieve this, we solved the Bethe-Salpeter Equation (BSE)³⁷, which includes both local-field effects and screened electron–hole attraction. The BSE can be reformulated as an eigenvalue problem, which is defined by a two-particle Hamiltonian^{34,38} written on a basis of electron–hole transitions $t = (n_1\mathbf{k}_1) \rightarrow t' = (n_2\mathbf{k}_2)$. In this work, we solved the BSE in the Tamm-Dancoff approximation, including therefore only resonant transitions, $(v, \mathbf{k} - \mathbf{q}) \rightarrow (c, \mathbf{k})$, where the momentum $\mathbf{q} = \mathbf{k}_2 - \mathbf{k}_1$ is in

the first Brillouin zone (v and c denoting valence and conduction bands, respectively). The matrix elements of the BSE are written in the following manner:

$$\langle t' | H_{exc}(\mathbf{q}) | t \rangle = E_t \delta_{t,t'} + \langle t' | \bar{V} - W | t \rangle \quad (2)$$

where E_t is the energy associated with the above mentioned transition from valence to conduction, \bar{V} is the Coulomb potential derived from the variation of the Hartree term, and W is the screened electron–hole interaction derived from the screened exchange.³⁷ The energies that enter the BSE include the quasiparticle corrections calculated within the G_0W_0 approximation. After diagonalization of Eq. 2 we obtain the eigenvectors $A_{cv\mathbf{k}}^S(\mathbf{q})$ and eigenvalues $E_{\mathbf{q},\lambda}$ that are the eigenstates and the energies of the excitons (labeled by the index λ), the stationary state of the BSE. The exciton energies and wave-functions at $\mathbf{q} = 0$ are used to build up the macroscopic dielectric function (ε_M) as:

$$\varepsilon_M(\omega) = 1 - 4\pi \sum_{\lambda} \frac{|T_{\lambda}|^2}{\omega - E_{\mathbf{q}=0,\lambda} + i\eta}, \quad (3)$$

where $T_{\lambda} = \sum_{cv\mathbf{k}} d_{cv\mathbf{k}} A_{cv\mathbf{k}}^{\lambda}(\mathbf{q} = 0)$ are the excitonic dipoles, $d_{cv\mathbf{k}}$ are the dipole matrix elements between the Kohn-Sham states $d_{cv\mathbf{k}} = \langle v\mathbf{k} | \hat{r} | c\mathbf{k} \rangle$ and $i\eta$ is a small broadening term added to mimic the resolution of experimental spectra. To speed up convergence of the BSE with the number of k-points, we used the double-grid approach described in Ref. 39, see Sec II C for details.

A. Phonon-assisted light absorption

For the phonon-assisted absorption/emission, we follow the approach derived in Ref. 15 with two modifications. First, the phase of the exciton–phonon matrix elements has been fixed using the code and the approach described in Ref. 40. Second, the definition of phonon-assisted transition dipoles has been corrected to be gauge consistent. This corresponds to including also the off-diagonal matrix elements of the exciton-phonon self-energy of Ref. 15. Then, the first order correction to the dielectric constant Eq. 3 induced by the coupling with phonons can be written as:

$$\Delta\varepsilon_M(\omega) = \sum_{\lambda\mu\beta\mathbf{q}} |T_{\lambda} \mathcal{D}_{\beta\lambda,\mathbf{q}\mu}^{\pm}|^2 \frac{1/2 \pm 1/2 + n_{\mathbf{q},\mu}}{\omega - E_{\mathbf{q},\beta} \pm \omega_{\mathbf{q}\mu} + i\eta} \quad (4)$$

here, T_{λ} are the excitonic dipoles and $\mathcal{D}_{\beta\lambda,\mathbf{q}\mu}^{\pm}$ are the phonon-assisted coupling dipole moments. Eq. 4 describes the satellites generated by the emission or absorption of phonons by an exciton, and they appear as a peak at the energy of the finite-momentum excitons $E_{\mathbf{q},\beta}$ plus or minus one phonon energy. The ‘ \pm ’ signs refer to phonon emission or absorption processes. The appearance of satellites also induces a renormalization of the purely exciton dielectric constant, a term that we do not consider here because the effect is small, and we investigate the two effects separately. For more details, see

Ref. 15 and 16. The phonon-assisted dipole moments can be written explicitly as

$$\mathcal{G}_{\beta\lambda,\mu\mathbf{q}}^{\pm} = \frac{\mathcal{G}_{\alpha\lambda}^{\mu\mathbf{q}}}{(E_{0\lambda} - E_{\mathbf{q}\beta} \pm \omega_{\mu\mathbf{q}} + i\eta)}. \quad (5)$$

where $\mathcal{G}_{\alpha\lambda}^{\mu\mathbf{q}}$ are the exciton–phonon coupling matrix elements at momentum \mathbf{q} ^{15,16} (since luminescence is always mediated by the recombination of an intermediate optical exciton, \mathcal{G} depends on a single momentum \mathbf{q} corresponding to the phonon momentum). The small imaginary part η in the phonon-assisted dipole moments derives from the exciton–phonon self-energy, see Ref. 15. We set its value to 1 meV,

$$I_{PL}^{(1)}(\omega; T) \propto \frac{1}{N_{\mathbf{q}}} \sum_{s,\mu,\beta,\mathbf{q}} \left| \sum_{\lambda} \frac{T_{\lambda}^* (\mathcal{G}_{\beta\lambda}^{\mu\mathbf{q}})^*}{E_{\mathbf{q}\beta} - E_{\lambda} - s\omega_{\mu\mathbf{q}} - i\eta} \right|^2 N_{\beta\mathbf{q}}(T_{\text{exc}}) F_{\mu\mathbf{q}}^s(T) \delta(\omega - [E_{\mathbf{q}\beta} - s\omega_{\mu\mathbf{q}}]). \quad (6)$$

In this equation, the oscillator strength of the peak is given by the exciton–phonon coupling matrix elements $\mathcal{G}_{\alpha\lambda}^{\mu\mathbf{q}}$ multiplied by the exciton dipoles T_{λ} . Here E_{λ} and $E_{\beta\mathbf{q}}$ are the energies of the optical and finite-momentum excitons, respectively, while $\omega_{\mu\mathbf{q}}$ are the phonon energies. The occupation function F is

$$F_{\mu\mathbf{q}}^s(T) = N_{\mu\mathbf{q}}(T) + \frac{1+s}{2}. \quad (7)$$

Here, $N_{\mu\mathbf{q}}(T)$ is the temperature-dependent phonon Bose-Einstein occupation function. As can be seen, $s = 1$ corresponds to processes of phonon “emission” ($\propto N_{\mu\mathbf{q}}(T) + 1$) — the integer value representing spontaneous phonon emission also at $T = 0$ — while $s = -1$ corresponds to processes of phonon “absorption” ($\propto N_{\mu\mathbf{q}}(T)$). Therefore, $I_{PL}^{(1)}(\omega; T)$ describes “light” emission by recombining excitons mediated by either “phonon” absorption or emission.

Luminescence is technically an out-of-equilibrium process, but we can assume that for a very low density of excitations and in steady-state conditions, the exciton population can be approximately described by an equilibrium distribution evaluated at an effective temperature T_{exc} . Here, we use the Boltzmann distribution. Experimentally, T_{exc} tends to coincide with the lattice temperature T more or less above 100 K, while at very low temperature (< 10 K), T_{exc} may vary between 10–50 K. The parameter T_{exc} is an effective excitonic temperature, used in the Boltzmann distribution to model excitonic occupations. Finally, in a real luminescence calculation, we replace the delta function in Eq. (6) by a Lorentzian, with a smearing set to 0.025 eV.

C. Computational details

Ground state properties of the Kohn-Sham bandstructure were obtained using the Quantum-Espresso (QE) code³² us-

which is large enough to remove unphysical divergences and small enough not to affect the final optical spectrum. In this work, we treat the bound exciton as a well-defined quasiparticle and therefore ignore possible overscreening effects.^{41,42} This approximation has been shown to be excellent in previous studies on BN systems.

B. Phonon assisted luminescence

To apply Eqs. (3) and (4) to the light emission process, we use a steady-state approximation to obtain the luminescence via the van Roosbroeck-Shockley (RS) relation^{28,43,44}:

ing DOJO norm-conserving pseudo-potentials⁴⁵ and PBE-sol exchange correlation functional⁴⁶ and a cutoff for the wavefunctions of 80 Ry. The phonons were also calculated with the QE code, using a $12 \times 12 \times 12$ k-grid and a $12 \times 12 \times 12$ q-grid.

GW and BSE calculations were performed using the Yambo code³⁵. We used a cutoff of 6 Ha and 80 bands for the dielectric constant, and the same number of bands to expand the Green’s function. In the Bethe-Salpeter equation, we included 3 valence and 3 conduction bands. To speed up convergence with k-point, we used the double-grid method as implemented in Ref. 39 with the fine k-point grid of $61 \times 61 \times 61$ k-points. Exciton–phonon coupling matrix elements were calculated using YamboPy⁴⁷ and the LetzElPhC library⁴⁸ using the same band range of the BSE and the same q-grid. The symmetry and selection rule analysis⁴⁰ was also performed with Yambopy via the spglib⁴⁹ and MolSym⁵⁰ packages.

In the calculation of phonon-assisted light absorption, exciton and phonon energies are interpolated on a large q-grid $61 \times 61 \times 61$ and used in the double-grid version of Eqs. (4) and (6) as described in Appendix A of Ref. 15. In particular, phonon energies were interpolated using force constants from QE³² while excitons were interpolated on the same q-grid using a smooth Fourier interpolation.⁵¹ For the calculation of the phonon-assisted dielectric constant we included the lowest 9 excitonic states and we include 20 scattering states in the sum of Eq. 3, that is enough to converge the phonon-assisted absorption/emission, in the luminescence spectrum we consider an excitonic and phononic temperature of 10 K, corresponding to the occupation of the deep minimum of the exciton dispersion.

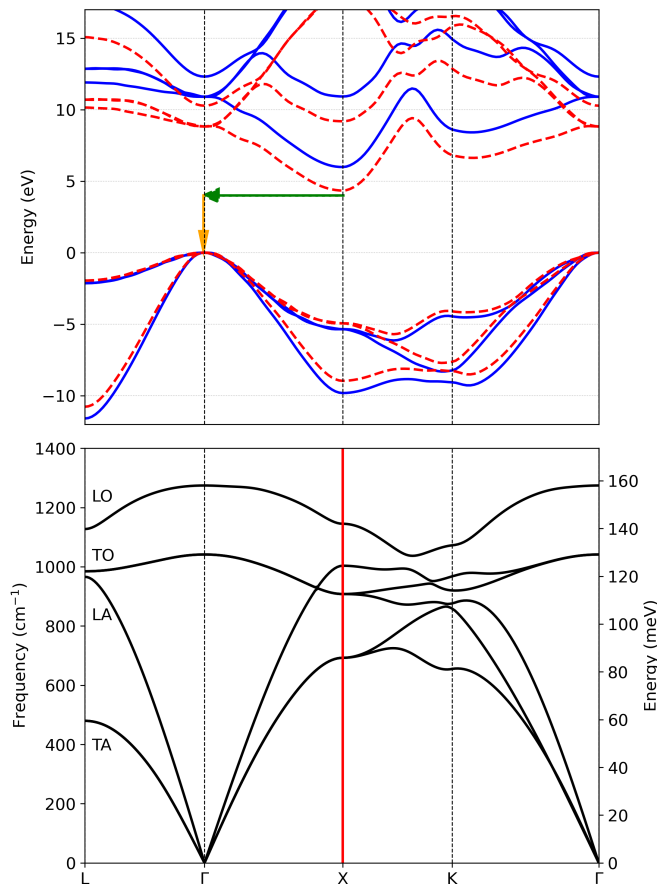


FIG. 1. In the top panel, we show the electronic band structure calculated at the Kohn-Sham (KS) (dashed red line) and G_0W_0 (solid blue line) approximation. In the same panel, we also show the lowest phonon-assisted transitions, with the green (phonon-emission) and orange (photon-emission) arrows. In the bottom panel, we show the phonon bandstructure, and we indicate in red the phonons at $\mathbf{q} = X$ that are responsible for the lowest phonon-assisted transitions between valence and conduction bands.

III. RESULTS

In this section, we present the results for the various properties of *c*BN.

A. Electronic and phononic bandstructures

In the top panel of Fig. 1, we report the bandstructure of *c*BN calculated at the KS and G_0W_0 level. We find the direct band gap at Γ of 8.82 eV and 10.91 eV at DFT and G_0W_0 levels. The indirect gap between $\Gamma - X$ is 4.34 eV and 6.0 eV. These values have to be compared with results from S. Louie et al.²⁴ who found 4.3 eV and 6.3 eV for the indirect and 8.6 eV and 11.4 eV for the direct one. G. Satta et al. found 11.4 eV for the direct band gap²⁶ and experiments report 6.4 ± 0.5 and 14.5 eV⁵². In general we expect our GW correction to be smaller than the one obtained from the S.

Louie et al. due to the different plasmon-pole model (for a discussion see Ref. 36), while regarding the comparison with G. Satta et al. two factors can explain the difference: first, we used the experimental lattice constant while they optimized it in DFT, and second, the parameters of our calculations are much more converged. Regarding the experimental result, it must be considered with great uncertainty, given that it is a marginal result with respect to the main aim of that work.

In general, it is well known that in large band gap materials G_0W_0 tends to underestimate the gap correction and usually self-consistency improves the agreement with the experiments⁵³. However, in this work, we decided to stick with the G_0W_0 +BSE approximation in order to be consistent with other works in the literature and on the assumption that any possible error in this approximation is of the same order in all BN polymorphs, so that we can compare our results with others on similar materials. We also neglect all energy renormalizations due to electron-phonon interactions, namely quasiparticle band-gap reduction and exciton binding energy increase, which partially compensate. In summary, our results should be interpreted with the understanding that certain physical effects, mostly pertaining to the absolute energy position of the optical spectra, are not taken into account, while they provide a good description of the optical response of *c*BN as far as coupling strengths and relative energy positions are concerned.

In the bottom panel of Fig. 1, we report the phonon bandstructure calculated with Density Functional Perturbation Theory (DFPT) as implemented in the QE code. With the same approach, we also calculated the deformation potential that enters into the definition of the electron-phonon and then the exciton-phonon matrix elements. We found an LO-TO splitting at Γ of 29 meV and the overall phonon bands are in good agreement with experimental measurements^{54,55} and previous calculations⁵⁶.

B. Optical properties and exciton dispersion

Starting from the quasiparticle bandstructure calculated in the previous section, we solved the Bethe-Salpeter equation (Eq. (2)). Then we calculated the optical absorption of *c*BN according to Eq. 3. In agreement with previous studies²⁶, we found that the optical response of *c*BN requires a very dense grid to converge. For this reason, we repeated the calculation using the Haydock technique (an iterative solver) combined with a double-grid approach³⁹ to obtain smoother spectra. In Fig. 2 we report the BSE results compared with the independent particle approximation (IPA) starting from the KS bandstructure.

We found that the onset of absorption begins at around 10.5 eV, at much higher energies than those reported in experiments. In Fig. 2 we have also indicated the first two absorption peaks with letters A and B, the first being a bound state with binding energy of approximately 0.3 eV and the second above the G_0W_0 gap. Compared to the IPA, the combination of GW+BSE shifts the spectrum, and several bound excitonic states form. However, the situation is quite

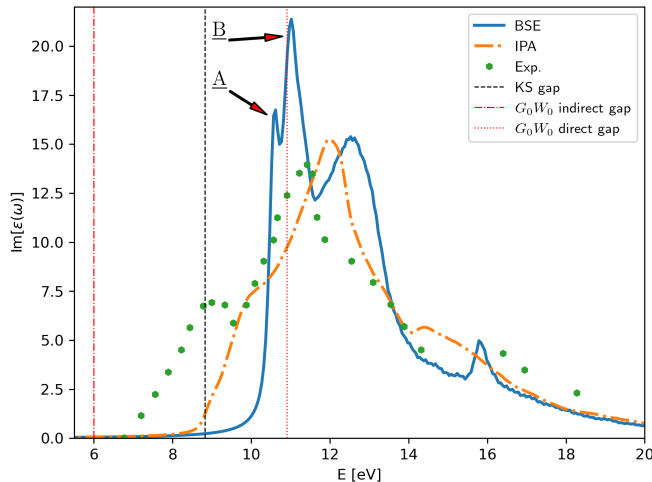


FIG. 2. Optical absorption of cBN calculated at the Bethe-Salpeter equation (BSE, solid blue line) and independent particle approximation (IPA, dot-dashed orange line) levels. In the figure, we have indicated the first two peaks of the spectrum with A and B. Results are compared with experimental measurements from Ref. 57. In the same figure, we also report the direct KS (black dashed line) and the direct and indirect G_0W_0 gaps (red dash-dotted lines and dotted lines).

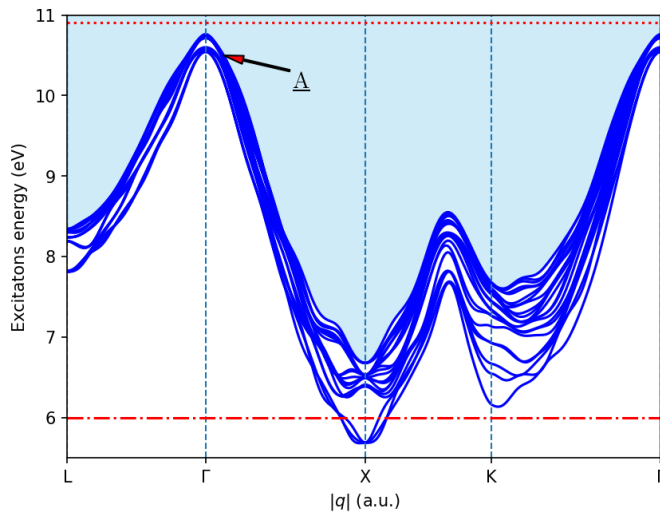


FIG. 3. Excitonic dispersion of cBN for the first lowest 20 excitons along the high-symmetry points of the Brillouin Zone. Excitonic bands are interpolated using a smooth Fourier transform.⁵¹ We report also the position of the 3 times degenerate exciton states responsible for the first absorption peak A at the Γ point (see Fig. 2) and the direct KS (black dashed line) and the direct and indirect G_0W_0 gaps (red dash-dotted lines and dotted lines).

different from that of hBN, where all the spectral weight is concentrated in a few excitonic states⁵⁸. In the cBN case, the spectrum is the sum of many excitonic states with close energies. This is clearly visible when the excitonic dispersion is plotted. To do this, we solved BSE at finite momentum on a

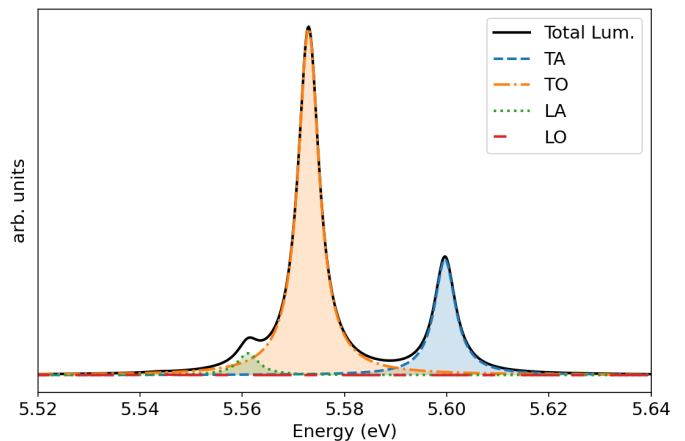


FIG. 4. Total phonon-assisted luminescence of cBN (continuous line) and the contribution of the different phonon modes at $q = X$: LO branch (red loosely dashed line), LA branch (green dotted line), TO branch (orange dot-dashed line), TA branch (blue dashed line).

regular q -grid (see Sec. II C). In Fig. 3, we report the exciton dispersion along high-symmetry lines. The indirect nature of cBN is clearly visible: in particular, the Γ point (corresponding to the optical limit) does not lie at the bottom of a valley, but instead is one of the highest energy points in the bands. Here, we have a low-energy subset of 9 exciton states between 10.54 and 10.6 eV. The first absorption peak visible in Fig. 2, denoted as ‘A’, lies in this subset: it is three times degenerate and transforms as the T_2 representation of the T_d point group of cBN (only states with this symmetry satisfy the optical selection rules and can be bright). Furthermore, the LT splitting of this state - verified by solving the BSE at $q = 0$ with and without the long-range part of the Coulomb interaction - amounts to 0.05 eV (the longitudinal state jumps from 10.55 to 10.6 eV). There is also a dark T_1 triplet lying 15 meV below the A peak, while the remainder of the 9-state subset is composed by a doubly degenerate state (E) and a nondegenerate one (A_1). The minimum of the excitonic dispersion is located at the X point at 5.685 eV, almost 5 eV below the Γ point, consistent with the deep indirect nature of the electronic gap. Here, the minimum is formed by three states: first, a doubly degenerate state transforming as the E representation of the little group D_{2d} of the X point, followed 5 meV above by a nondegenerate A_1 state.

C. Phonon-assisted light absorption/emission

In Fig. 4 we report the phonon-assisted luminescence of cBN calculated using Eq. 6 at 10 K. At this temperature, the lowest-energy exciton (E) at $q = X$ is occupied, while the A_1 state above remains empty. Indeed, the luminescence originates from excitons at the X point. We found that the signal is centered around 5.55–5.6 eV, well below that of hBN (from 5.77–5.9 eV). In the same figure, we report the decomposition of the luminescence signal into the contribution of the differ-

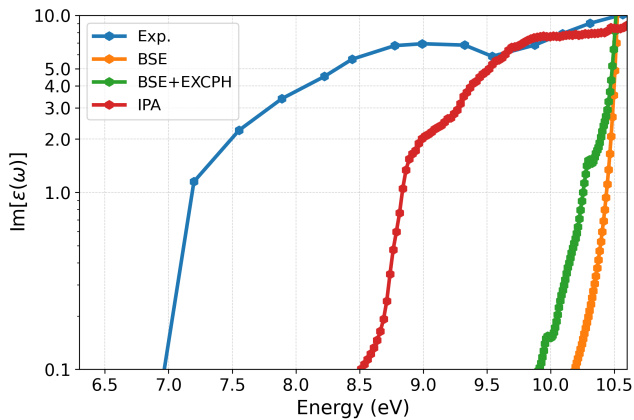


FIG. 5. Low energy tail of the optical absorption of cBN at different levels of approximation: independent particle approximation (IPA), Bethe-Salpeter (BSE), and Bethe-Salpeter plus exciton-phonon coupling (BSE-EXCPH). Results are compared with experimental measurements from Ref. 57.

ent phonon modes. To interpret the luminescence spectrum, we refer to the X phonons shown in the lower panel of Fig. 1, highlighted by a vertical red line in the same figure. These are the phonon modes that match the momentum of the lowest excitonic states in Fig. 3. In order to distinguish the different phonon modes we use the same nomenclature as for Γ phonons, as it is clear from the continuous lines of the phonon dispersion which mode we are referring to. Combining all this information we found that phonon-assisted transitions are primarily mediated by transverse phonon branches with a small contribution of longitudinal branches at lower energies. For the E exciton, it is important to emphasize that the selection rules for the phonon-mediated recombination process (which requires a bright T_2 exciton as final state, see Eq. 6) allow for coupling with any phonon mode. Instead, in the case of the A_1 exciton, the coupling with the mode corresponding to the ‘LA’ branch is forbidden.

Compared to the more famous and better characterized luminescence spectrum of hBN^{3,27,28}, the spectrum of cBN presents several differences: firstly, it is located at a lower energy; secondly, longitudinal and transverse phonons at X are not so separate as in hBN to generate a doublet in luminescence; thirdly, unlike hBN, the phonon modes that contribute most are from the ‘TO’ and ‘TA’ branches, while ‘LA’ and ‘LO’ are low or irrelevant. All these characteristics will make it possible to distinguish it in future experiments on clean samples of cBN.

Finally, in Fig. 5 we report the low energy tail of the dielectric function including the contribution from the exciton-phonon scattering obtained from Eq. 4 interpolated on a double-grid for exciton and phonon energies¹⁵ at 10 K. We found that coupling with phonons red-shifts the onset from 10.3 to 9.8 eV. Looking at the excitonic dispersion, Fig. 3, one would expect even a lower energy contribution of the epsilon. However, transitions toward low excitons close to X have a very weak intensity due to the large denominators that appear in Eq. 5. For this reason, the first visible contribution to the epsilon is

only 1 eV below the direct transitions.

IV. CONCLUSIONS

In this work, we have investigated the optical response of cubic boron nitride (cBN) using first-principles many-body perturbation theory, specifically accounting for the critical role of exciton-phonon coupling. Our findings provide a better understanding of the long-standing discrepancy between theoretical predictions of a ~ 11 eV optical gap and experimental reports of absorption and emission features in the 6-7 eV range. We have shown that while the direct optical gap remains high, the inclusion of exciton-phonon interactions effectively lowers the observable absorption onset. However, intrinsic exciton-phonon coupling in the pristine system is not enough to reconcile theory with experimental observations. In fact, even if excitons at very low energy are present in cBN, their contribution to the dielectric constant is suppressed by the large denominators in the phonon-assisted dipoles. We expect that the low-energy contribution in the experimental measurement of the dielectric constant of cBN is due to the presence of defects, through direct transition to defect levels or to the activation of transition to finite momentum excitons due to the breaking of translation symmetry⁵⁹.

Regarding the luminescence, our results show that cBN and hBN exhibit distinct spectral profiles. We found that the intrinsic phonon-assisted luminescence of pure cBN is centered around 5.57–5.60 eV, which is lower than that typically observed for hBN, from 5.77–5.9 eV. This energy shift suggests that experimental emission signals reported around 6 eV may be attributed to hBN inclusions within cBN samples rather than the intrinsic cBN or defect-related states. This underscores the sensitivity of luminescence spectroscopy as a tool for phase characterization in boron nitride polymorphs.

ACKNOWLEDGMENTS

C.A. and A.P. acknowledge B. Demoulin and A. Saul for the management of the computer cluster *Claudia*. F.P. acknowledges Muralidhar Nalabothula for insightful discussions on exciton symmetries and the evaluation of luminescence spectra. C.A. acknowledges funding from European Research Council MSCA-ITN TIMES under grant agreement 101118915. E.C. acknowledges ANR project COLIBRI No. ANR-22-CE30-0027. C.A., A.M. and A.P. acknowledge support from the Amidex foundation through the project INDIGENA. F.P. Acknowledges support from ICSC - Centro Nazionale di Ricerca in High Performance Computing, Big Data and Quantum Computing - funded by the European Union through the Italian Ministry of University and Research under PNRR M4C2I1.4 (Grant No. CN0000013). This work has also been supported by the European Union through the MaX “MAterials design at the eXascale” Centre of Excellence (Grant agreement No. 101093374, co-funded by the EuroHPC JU).

- ¹C. Cazorla and T. Gould, *Science Advances* **5**, eaau5832 (2019), <https://www.science.org/doi/pdf/10.1126/sciadv.aau5832>.
- ²P. Jaffrennou, J. Barjon, J.-S. Lauret, B. Attal-Trétout, F. Ducastelle, and A. Loiseau, *Journal of Applied Physics* **102** (2007).
- ³M. Zanfrognini, A. Plaud, I. Stenger, F. Fossard, L. Sponza, L. Schué, F. Paleari, E. Molinari, D. Varsano, L. Wirtz, F. m. c. Ducastelle, A. Loiseau, and J. Barjon, *Phys. Rev. Lett.* **131**, 206902 (2023).
- ⁴P. Lechiffart, F. Paleari, and C. Attaccalite, *SciPost Phys.* **12**, 145 (2022).
- ⁵L. Schué, “Propriétés optiques et structurales du nitrure de bore en hybridation sp^2 : des cristaux massifs aux feuillets atomiques,” <https://tel.archives-ouvertes.fr/tel-01827237/> (2017), ph.D. thesis, Université Paris-Saclay.
- ⁶G. Cassaboïs, A. Rousseau, C. Elias, T. Pelini, P. Vuong, P. Valvin, and B. Gil, *Comptes Rendus. Physique* **22**, 1 (2021).
- ⁷L. Schué, L. Sponza, A. Plaud, H. Bensalah, K. Watanabe, T. Taniguchi, F. Ducastelle, A. Loiseau, and J. Barjon, *Phys. Rev. Lett.* **122**, 067401 (2019).
- ⁸C. Elias, G. Fugallo, P. Valvin, C. L’Henoret, J. Li, J. Edgar, F. Sottile, M. Lazzeri, A. Ouerghi, B. Gil, *et al.*, *Physical Review Letters* **127**, 137401 (2021).
- ⁹G. Cassaboïs, P. Valvin, and B. Gil, *Nature Photonics* **10**, 262 (2016).
- ¹⁰L. Schué, L. Sponza, A. Plaud, H. Bensalah, K. Watanabe, T. Taniguchi, F. m. c. Ducastelle, A. Loiseau, and J. Barjon, *Phys. Rev. Lett.* **122**, 067401 (2019).
- ¹¹C. Elias, G. Fugallo, P. Valvin, C. L’Henoret, J. Li, J. H. Edgar, F. Sottile, M. Lazzeri, A. Ouerghi, B. Gil, and G. Cassaboïs, *Phys. Rev. Lett.* **127**, 137401 (2021).
- ¹²M. Silvetti, C. Attaccalite, and E. Cannuccia, *Phys. Rev. Mater.* **7**, 055201 (2023).
- ¹³A. Rousseau, J. Plo, P. Valvin, T. S. Cheng, J. Bradford, T. James, J. Wrigley, C. Mellor, P. Beton, S. Novikov, *et al.*, *2D Materials* **11**, 025026 (2024).
- ¹⁴L. Y. Liu, S. Y. Woo, J. Wu, B. Hou, C. Su, and D. Y. Qiu, *arXiv preprint arXiv:2502.20454* (2025).
- ¹⁵P. Lechiffart, F. Paleari, D. Sangalli, and C. Attaccalite, *Phys. Rev. Mater.* **7**, 024006 (2023).
- ¹⁶G. Marini, M. Calandra, and P. Cudazzo, *Nano Letters* **24**, 6017 (2024).
- ¹⁷L. Fu, Y. Hu, N. Tang, J. Duan, X. Jia, H. Yang, Z. Li, X. Han, G. Li, J. Lu, L. Dai, W. Ge, Y. Yao, and B. Shen, *Phys. Rev. Lett.* **135**, 046903 (2025).
- ¹⁸C. Samantary and R. Singh, *International Materials Reviews* **50**, 313 (2005).
- ¹⁹P. Mirkarimi, K. McCarty, and D. Medlin, *Materials Science and Engineering: R: Reports* **21**, 47 (1997).
- ²⁰A. Onodera, M. Nakatani, M. Kobayashi, Y. Nisida, and O. Mishima, *Physical Review B* **48**, 2777 (1993).
- ²¹N. Miyata, K. Moriki, O. Mishima, M. Fujisawa, and T. Hattori, *Physical Review B* **40**, 12028 (1989).
- ²²S. Galambosi, J. Soininen, K. Hämäläinen, E. L. Shirley, and C.-C. Kao, *Physical Review B* **64**, 024102 (2001).
- ²³V. Sobolev and M. Zlobina, *Journal of Applied Spectroscopy* **66**, 654 (1999).
- ²⁴M. P. Surh, S. G. Louie, and M. L. Cohen, *Phys. Rev. B* **43**, 9126 (1991).
- ²⁵G. Cappellini, G. Satta, M. Palumbo, and G. Onida, *Physical Review B* **64**, 035104 (2001).
- ²⁶G. Satta, G. Cappellini, V. Olevano, and L. Reining, *Physical Review B—Condensed Matter and Materials Physics* **70**, 195212 (2004).
- ²⁷E. Cannuccia, B. Monserrat, and C. Attaccalite, *Phys. Rev. B* **99**, 081109 (2019).
- ²⁸F. Paleari, H. P.C.Miranda, A. Molina-Sánchez, and L. Wirtz, *Phys. Rev. Lett.* **122**, 187401 (2019).
- ²⁹S. Iqbal, T. Cheng, X. Duan, L. Liu, and J.-Y. Yang, *Journal of Applied Physics* **135** (2024).
- ³⁰S. N. Shirodkar, C. A. Sayou Ngoms, and P. Dev, *ACS Applied Electronic Materials* **5**, 1707 (2023).
- ³¹S. Zhu, L. Hu, Z. Lin, X. Wei, J. He, and W. Zheng, *ACS Photonics* **11**, 286 (2023).
- ³²P. Giannozzi, O. Andreussi, T. Brumme, O. Bunau, M. B. Nardelli, M. Calandra, R. Car, C. Cavazzoni, D. Ceresoli, M. Cococcioni, N. Colonna, I. Carnimeo, A. D. Corso, S. de Gironcoli, P. Delugas, R. A. DiStasio, A. Ferretti, A. Floris, G. Fratesi, G. Fugallo, R. Gebauer, U. Gerstmann, F. Giustino, T. Gorni, J. Jia, M. Kawamura, H.-Y. Ko, A. Kokalj, E. Küçbenli, M. Lazzeri, M. Marsili, N. Marzari, F. Mauri, N. L. Nguyen, H.-V. Nguyen, A. O. de-la Roza, L. Paulatto, S. Poncé, D. Rocca, R. Sabatini, B. Santra, M. Schlipf, A. P. Seitsonen, A. Smogunov, I. Timrov, T. Thonhauser, P. Umari, N. Vast, X. Wu, and S. Baroni, *Journal of Physics: Condensed Matter* **29**, 465901 (2017).
- ³³E. Knittle, R. M. Wentzcovitch, R. Jeanloz, and M. L. Cohen, *Nature* **337**, 349 (1989).
- ³⁴R. M. Martin, L. Reining, and D. M. Ceperley, *Interacting electrons* (Cambridge University Press, 2016).
- ³⁵D. Sangalli, A. Ferretti, H. Miranda, C. Attaccalite, I. Marri, E. Cannuccia, P. Melo, M. Marsili, F. Paleari, A. Marrazzo, *et al.*, *Journal of Physics: Condensed Matter* **31**, 325902 (2019).
- ³⁶M. Stankovski, G. Antonius, D. Waroquiers, A. Miglio, H. Dixit, K. Sankaran, M. Giantomassi, X. Gonze, M. Côté, and G.-M. Rignanese, *Phys. Rev. B* **84**, 241201 (2011).
- ³⁷G. Strinati, *Riv. Nuovo Cimento* **11**, 1 (1988).
- ³⁸M. Gatti and F. Sottile, *Phys. Rev. B* **88**, 155113 (2013).
- ³⁹I. M. Allati, D. Sangalli, and M. Grüning, *Frontiers in Chemistry* **9**, 763946 (2022).
- ⁴⁰M. Nalobothula, *Symmetries of Excitons: Implications for Exciton-Phonon Coupling and Optical Spectroscopy*, Ph.D. thesis, Unilu - Université du Luxembourg [The Faculty of Science, Technology and Medicine], Luxembourg, Luxembourg (12 May 2025), <https://orbilu.uni.lu/10993/65236>.
- ⁴¹F. Paleari and A. Marini, *Phys. Rev. B* **106**, 125403 (2022).
- ⁴²G. Stefanucci and E. Perfetto, *SciPost Phys.* **18**, 009 (2025).
- ⁴³W. Van Roosbroeck and W. Shockley, *Physical Review* **94**, 1558 (1954).
- ⁴⁴H. B. Bebb and E. W. Williams, *Semiconductors and semimetals* (Elsevier, 1972) Chap. Photoluminescence I: Theory.
- ⁴⁵M. van Setten, M. Giantomassi, E. Bousquet, M. Verstraete, D. Hamann, X. Gonze, and G.-M. Rignanese, *Computer Physics Communications* **226**, 39 (2018), <http://www.pseudo-djojo.org/>.
- ⁴⁶J. P. Perdew, A. Ruzsinszky, G. I. Csonka, O. A. Vydrov, G. E. Scuseria, L. A. Constantin, X. Zhou, and K. Burke, *Physical review letters* **100**, 136406 (2008).
- ⁴⁷F. Paleari, A. Molina-Sánchez, M. Nalobothula, R. Reho, M. Bonacci, J. M. Castelo, J. Cervantes-Villanueva, M. Pionteck, M. Silvetti, C. Attaccalite, and H. Pereira Coutada Miranda, “YamboPy,” (2025).
- ⁴⁸LetzEIPhC, “Lätzebuerg Electron Phonon Code,” <https://gitlab.com/lumen-code/LetzEIPhC>.
- ⁴⁹A. Togo, K. Shinohara, and I. Tanaka, *Science and Technology of Advanced Materials: Methods* **4**, 2384822 (2024), <https://doi.org/10.1080/27660400.2024.2384822>.
- ⁵⁰S. M. Goodlett, N. L. Kitzmiller, J. M. Turney, and I. Schaefer, Henry F., *The Journal of Chemical Physics* **161**, 024107 (2024), https://pubs.aip.org/aip/jcp/article-pdf/doi/10.1063/5.0216738/20039263/024107_1_5.0216738.pdf.
- ⁵¹W. E. Pickett, H. Krakauer, and P. B. Allen, *Phys. Rev. B* **38**, 2721 (1988).
- ⁵²H. R. Philipp and E. A. Taft, *Phys. Rev.* **127**, 159 (1962).
- ⁵³L. Artús, M. Feneberg, C. Attaccalite, J. H. Edgar, J. Li, R. Goldhahn, and R. Cuscó, *Advanced Photonics Research* **2**, 2000101 (2021).
- ⁵⁴Y. Cai, L. Zhang, Q. Zeng, L. Cheng, and Y. Xu, *Solid state communications* **141**, 262 (2007).
- ⁵⁵M. Eremets, M. Gauthier, A. Polian, J. Chervin, J. Besson, G. Dubitskii, and Y. Y. Semenova, *Physical Review B* **52**, 8854 (1995).
- ⁵⁶N. Ohba, K. Miwa, N. Nagasako, and A. Fukumoto, *Phys. Rev. B* **63**, 115207 (2001).
- ⁵⁷J. J. Pouch and S. A. Alterovitz, in *Materials Science Forum*, Vol. 54 (Trans Tech Publications Ltd, 1990) p. 165.
- ⁵⁸F. Paleari, T. Galvani, H. Amara, F. Ducastelle, A. Molina-Sánchez, and L. Wirtz, *2D Materials* **5**, 045017 (2018).
- ⁵⁹A. Tararan, S. Di Sabatino, M. Gatti, T. Taniguchi, K. Watanabe, L. Reining, L. Tizei, M. Kociak, and A. Zobelli, *Physical Review B* **98**, 094106 (2018).